

TRANSFERRED THIN FILM LITHIUM NIOBATE AS MILLIMETER WAVE ACOUSTIC FILTER PLATFORMS

Omar Barrera¹, Sinwoo Cho¹, Kenny Hyunh², Jack Kramer¹, Michael Liao²
Vakhtang Chulukhadze¹, Lezli Matto², Mark S. Goorsky², and Ruochen Lu¹

¹University of Texas at Austin, and ²University of California Los Angeles

ABSTRACT

This paper reports the first high-performance acoustic filters toward millimeter wave (mmWave) bands using transferred single-crystal thin film lithium niobate (LiNbO₃). By transferring LiNbO₃ on the top of silicon (Si) and sapphire (Al₂O₃) substrates with an intermediate amorphous Si (aSi) bonding and sacrificial layer, we demonstrate compact acoustic filters with record-breaking performance beyond 20 GHz. In the LN-aSi-Al₂O₃ platform, the third-order ladder filter exhibits low insertion loss (IL) of 1.62 dB and 3-dB fractional bandwidth (FBW) of 19.8% at 22.1 GHz, while in the LN-aSi-Si platform, the filter shows low IL of 2.38 dB and FBW of 18.2% at 23.5 GHz. Material analysis validates the great crystalline quality of the stacks. The high-resolution x-ray diffraction (HRXRD) shows full width half maximum (FWHM) of 53" for Al₂O₃ and 206" for Si, both remarkably low compared to piezoelectric thin films of similar thickness. The reported results bring the state-of-the-art (SoA) of compact acoustic filters to much higher frequencies, and highlight transferred LiNbO₃ as promising platforms for mmWave filters in future wireless front ends.

KEYWORDS

Acoustic filters, lithium niobate, millimeter-wave, piezoelectric devices, thin-film devices.

INTRODUCTION

Mobile communication relies heavily on acoustic wave resonators for compact front-end filters in sub-6 GHz frequency bands [1]. Commercially successful acoustic filters can be mostly classified into two groups: surface acoustic wave (SAW) and bulk acoustic wave (BAW) devices [2], [3]. Both solutions share the same advantages of a small footprint compared to the electromagnetic (EM) counterparts, thanks to the short wavelengths of acoustics, suitable for handheld devices [4], [5]. As the demand for higher data rates increases, wireless communication is exploring millimeter wave (mmWave) frequency bands. Consequently, there is a growing need for compact filters at mmWave with low loss and great frequency selectivity [6], [7]. On the one hand, frequency-scaling acoustic filters have suffered excessive loss [Fig. 1 (a)] and bandwidth reduction [Fig. 1 (b)] due to a lack of high-performance mmWave acoustic resonator platforms [8]–[12]. On the other hand, circuit and EM solutions have disadvantages, such as the low Q of lumped components and the bulkiness of enclosures in cavity filters [13]. This work focuses on developing acoustic technologies for low-loss filter platforms at mmWave.

Increasing the operation frequencies of acoustic resonators is simple in principle, but maintaining device performance is challenging [14]. More specifically,

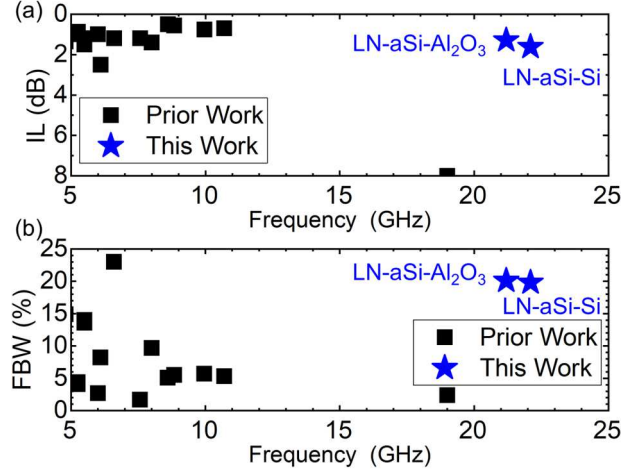


Fig. 1. Surveys indicating (a) IL and (b) FBW for reported acoustic filters with f_c beyond 5 GHz.

achieving simultaneously high quality factor (Q) and electromechanical coupling (k^2) at mmWave is difficult [15]–[22]. For SAW, reducing the electrode width translates to shorter wavelengths and higher frequencies, but this method is contingent on feature size (sub-100 nm) and thus limited by lithography [23], [24]. Besides, the routing resistance and self-inductance of interdigitated electrodes exacerbate for narrower electrodes. For BAW, the frequency is inversely proportional to the piezoelectric layer's thickness, while at mmWave, the film stack becomes significantly thin (sub-100 nm), causing challenges in maintaining piezoelectric film quality and lowering electrical loss [25]. Additionally, the resonators required to realize a 50 Ω matched filter must be very small to obtain the low values of static capacitance (C_0) required for the network, which inevitably results in lossy devices [6], [26]. Thus, a new piezoelectric acoustic platform at mmWave is needed.

Lately, alternate methods of exciting bulk acoustic waves in the thin film have resulted in laterally excited resonators on lithium niobate (LiNbO₃) operating in thickness-shear modes [27], [28]. Specifically, a new proposed stack involving transferred thin-film LiNbO₃ on low-loss substrates with an intermediate amorphous silicon layer has recorded resonators with impressive Q and k^2 [29], [30]. In this work, we exploit this material stack on 2 different carrier substrates, silicon (Si) and sapphire (Al₂O₃), demonstrating the capability of transferred film LiNbO₃ as a potential platform for mmWave acoustic filters. The fabricated devices exhibit low IL of 1.62 dB and 2.38 dB, with large FBW of 19.8% and 18.2% for the Si and Al₂O₃ substrates, respectively, elevating the current state of the art (Fig. 1). The third-order ladder filters are well matched to 50 Ω in a compact footprint of 0.56mm².

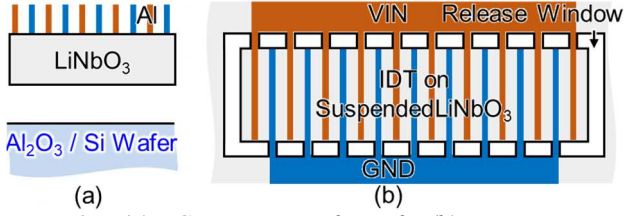


Fig. 2. (a) Cross-sectional and (b) top resonator schematics.

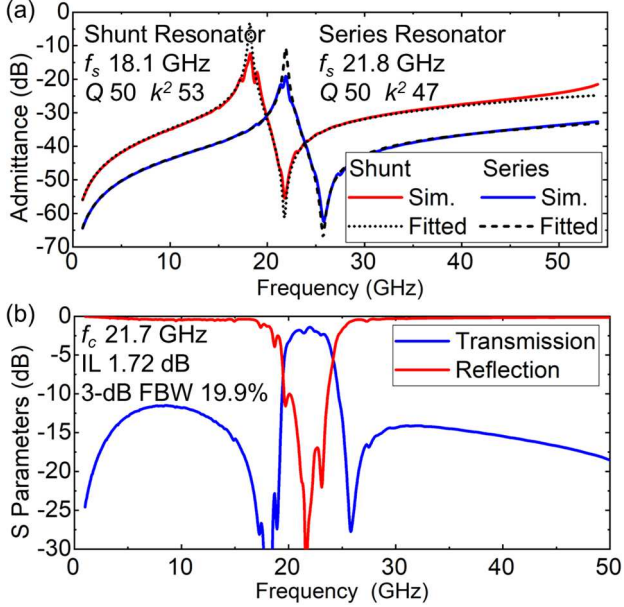


Fig. 3 (a) Simulated admittance, inset key specifications and vibration mode shape. (b) Simulated filter response.

These prototypes showcase a proof of concept as potential candidates for mmWave acoustic filters.

DESIGN AND SIMULATION

The cross-sectional and top views of the design are illustrated in Fig. 2. The active region consists of interdigitated transducers (IDT) on a thin-film LiNbO₃ piezoelectric layer. Thickness-shear waves, i.e., first-order antisymmetric (A1) mode, are excited via the e_{15} piezoelectric coefficient by the electrodes. Aluminum is selected for the metal layer with a thickness of 350 nm, and the spacing between electrodes is 3 μ m, following the guidelines reported in [29]. The design approach is identical for both Si and Al₂O₃ carrier substrates, as the resonators are released and only connected with the substrate with anchors. However, the difference between the two stacks lies in the EM feedthrough and transfer film quality (Figs. 4-5), which will be discussed later.

The resonator structure is validated using COMSOL finite element analysis, and the results are plotted in Fig. 3 (a). The results show a frequency shift, which is necessary for filter synthesis, where the parallel resonance (f_p) of the shunt resonator and the series resonance (f_s) of the series resonator are intended to overlap. This shift is achieved using different thicknesses of LiNbO₃ for the shunt and series resonators respectively. Q is set as 50 based on previously measured data, and k^2 is extracted as $k^2 = \pi^2/8 \cdot (f_p^2/f_s^2 - 1)$ from a fitting using the Butterworth-Van Dyke (MBVD) model [31]. The values of C_0 are

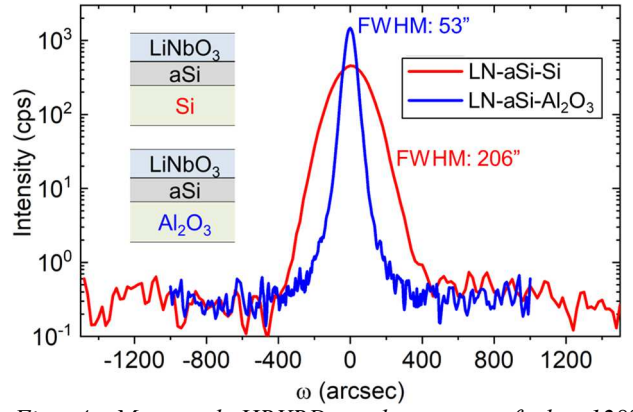


Fig. 4. Measured HRXRD rock curves of the 128° Y-cut LiNbO₃ crystal in both platforms show high crystal quality.

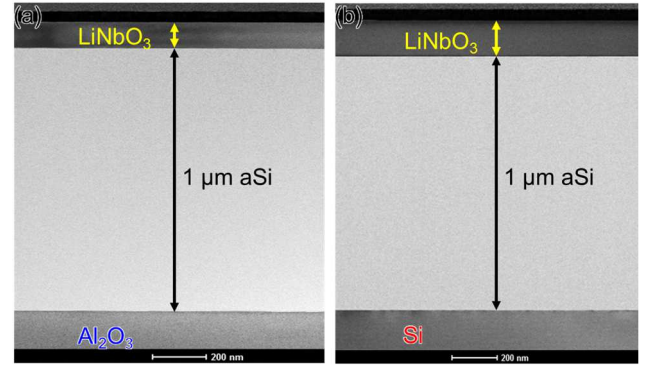


Fig. 5. Stack information measured with TEM pictures of (a) LN-aSi-Al₂O₃ and (b) LN-aSi-Si stacks.

selected to obtain minimum IL in a 50 Ω third-order ladder filter.

The obtained results are exported into a circuit simulator to assess the expected performance of the filter. The results [Fig. 3 (b)] show a filter centered at 21.7 GHz with IL of 1.72 dB and a 19.9% FBW, promising performance at this frequency range.

FABRICATION AND MEASUREMENT

The wafers used for this work were provided by NGK Insulators Ltd. The two proposed stacks (LN-aSi-Si & LN-aSi-Al₂O₃) are analyzed using material characterization techniques. First, rocking curves are measured using high-resolution x-ray diffraction (HRXRD) to validate the crystal quality of the material stacks (Fig. 4). The results show full width at half maximum (FWHM) of 53° for Al₂O₃ and 206° for Si, comparable to that reported in other thin film LiNbO₃ layers. Next, side profile images of the stack are measured using transmission electron microscopy (TEM). The results show clean interfaces between material boundaries, suggesting good crystallinity of the materials (Fig. 5). The images also reveal a slightly thicker LiNbO₃ layer for the LN-aSi-Si compared to the LN-aSi-Al₂O₃ stack, which suggests small thickness variations across the wafers.

The fabrication starts by trimming the LiNbO₃ thickness of the samples down to 90 nm, which provides the base start thickness used for the shunt resonators. The trimming is done using ion milling; in [27], the authors have validated good preservation of the crystal with this approach. Afterward, etching windows are patterned using

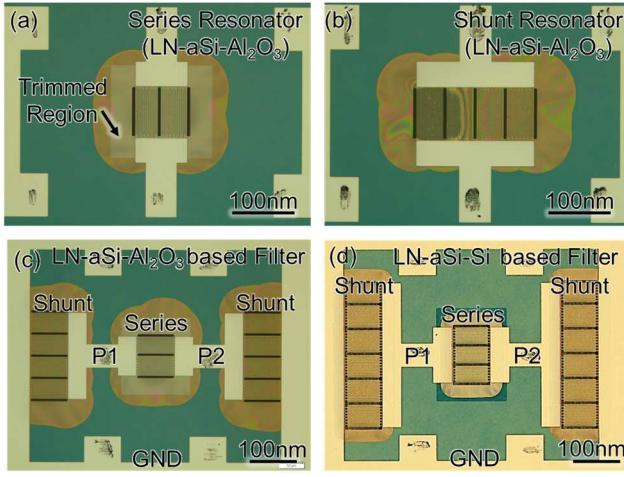


Fig. 6. Fabricated (a) series, (b) shunt resonator, and (c) filter in LN-aSi-Al₂O₃. (d) Filter in LN-aSi-Si.

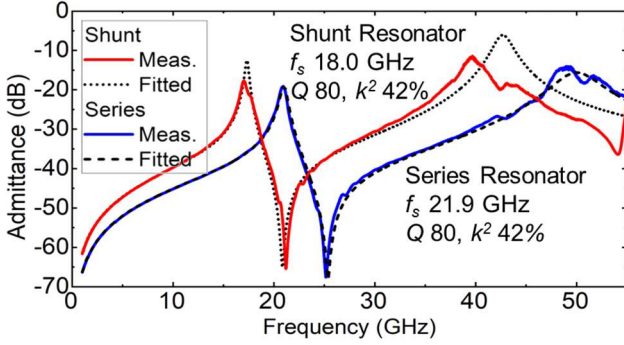


Fig. 7. Measured series & shunt resonator in LN-aSi-Al₂O₃.

lithography and etched into the aSi layer. The long lateral etch windows divide the devices into resonator banks, expediting the release process. Next, local regions for placement of the series resonators are defined using lithography. Afterward, a second round of ion milling is used on these exposed local trimming regions for a target thickness of 75 nm. The step height difference between these regions is accurately monitored using atomic force microscopy (AFM), with a measured height of 15 ± 1 nm. EBL lithography is used to pattern the fine features of the metal layer, and Al is evaporated for the metal deposition. The devices are then released by selectively etching the aSi intermediate layer using xenon difluoride (XeF₂). Figs. 6 (a)-(c) show optical images of the standalone resonators as well as the filter for the LN-aSi-Al₂O₃ sample and the LN-aSi-Si filter in Fig. 6(d).

The standalone resonators are measured at room temperature using a 67 GHz Keysight VNA. Fig. 7 shows the admittance response for the resonators on LN-aSi-Al₂O₃. The series and shunt devices exhibit nearly identical figures of merit, with k^2 of 42% and Q of 80. k^2 is extracted using MBVD and considering the series routing resistance and inductance observed in IDT devices. A good overlap between the f_p of the shunt resonator and the f_s of the shunt resonator can be observed around 22 GHz, corroborating the accuracy of the local trim.

The filter response for LN-aSi-Al₂O₃ (Fig. 8a) shows IL of 1.62 dB, FBW of 19.8% at 22.1 GHz f_c , whereas the LN-aSi-Si (Fig. 8b) sample has 2.38 dB IL with 18.2% FBW at f_c of 23.5 GHz. The measurements for filters and standalone resonators are in good agreement with the

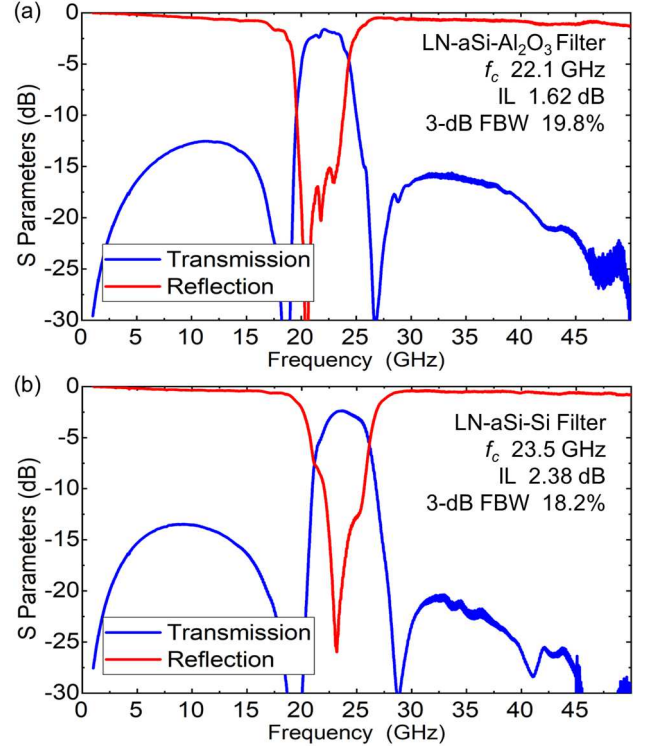


Fig. 8. Measured transmission and reflection of fabricated filters in (a) LN-aSi-Al₂O₃, and (b) LN-aSi-Si.

simulations, the discrepancy in f_c between the 2 filters is due to the small variations in the thickness of the LiNbO₃ layer across the sample surface. These results show remarkable frequency scaling and improved FBW compared to the SoA (Fig. 1) while maintaining low IL. The out-of-band characteristics are similar to other works using 3 resonator ladder filters [8], [32].

CONCLUSION

This work presents the suitability of transferred thin-film LiNbO₃ as a platform for mmWave filters. The prototypes show promising low-loss and wideband response, well above the current SoA. These unprecedented results are backed by material analysis, which shows excellent preservation of the piezoelectric layer crystal quality. The reported devices demonstrate the potential of transfer thin-film LiNbO₃ platforms as prospective candidates for the next generation of mmWave acoustic filters.

ACKNOWLEDGMENT

The authors thank the DARPA COFFEE program for funding support and Dr. Ben Griffin for helpful discussions.

REFERENCES

- [1] R. Ruby, "A Snapshot in Time: The Future in Filters for Cell Phones," *IEEE Microw Mag*, vol. 16, no. 7, pp. 46–59, 2015.
- [2] K. Hashimoto, *Surface Acoustic Wave Devices in Telecommunications*. 2000. doi: 10.1007/978-3-662-04223-6.
- [3] J. F. Rosenbaum, *Bulk Acoustic Wave Theory and Devices*. Artech House, 1988.
- [4] A. Hagelauer *et al.*, "From Microwave Acoustic Filters to Millimeter-Wave Operation and New

- Applications,” *IEEE Journal of Microwaves*, vol. 3, no. 1, pp. 484–508, 2023.
- [5] A. Link and P. Warder, “Golden age for filter design: Innovative and proven approaches for acoustic filter, duplexer, and multiplexer design,” *IEEE Microw Mag*, vol. 16, no. 7, 2015.
 - [6] R. Aigner, G. Fattinger, M. Schaefer, K. Karnati, R. Rothemund, and F. Dumont, “BAW filters for 5G bands,” in *2018 IEEE International Electron Devices Meeting (IEDM)*, IEEE, 2018, pp. 14–15.
 - [7] D. Kim *et al.*, “Wideband 6 GHz RF Filters for Wi-Fi 6E Using a Unique BAW Process and Highly Sc-doped AlN Thin Film,” in *2021 IEEE MTT-S International Microwave Symposium (IMS)*, 2021, pp. 207–209.
 - [8] Y. Yang, R. Lu, L. Gao, and S. Gong, “4.5 GHz Lithium Niobate MEMS Filters With 10% Fractional Bandwidth for 5G Front-Ends,” *Journal of Microelectromechanical Systems*, vol. 28, no. 4, pp. 575–577, 2019.
 - [9] L. Gao, Y. Yang, and S. Gong, “Wideband hybrid monolithic lithium niobate acoustic filter in the K-band,” *IEEE Trans Ultrason Ferroelectr Freq Control*, vol. 68, no. 4, pp. 1408–1417, 2020.
 - [10] G. Giribaldi, L. Colombo, P. Simeoni, and M. Rinaldi, “Compact and wideband nanoacoustic pass-band filters for future 5G and 6G cellular radios,” <https://doi.org/10.21203/rs.3.rs-2569732/v1>, Feb. 09, 2023.
 - [11] L. Zhang *et al.*, “High-Performance Acoustic Wave Devices on LiTaO₃/SiC Hetero-Substrates,” *IEEE Trans Microw Theory Tech*, pp. 1–11, 2023.
 - [12] Y. Yang, L. Gao, and S. Gong, “An X-band lithium niobate acoustic RFFE Filter with FBW of 3.45% and IL of 2.7 dB,” in *IEEE MTT-S International Microwave Symposium Digest*, 2020.
 - [13] R. V. Snyder, G. Macchiarella, S. Bastioli, and C. Tomassoni, “Emerging Trends in Techniques and Technology as Applied to Filter Design,” *IEEE Journal of Microwaves*, vol. 1, no. 1, pp. 317–344, 2021.
 - [14] S. Gong, R. Lu, Y. Yang, L. Gao, and A. E. Hassanien, “Microwave Acoustic Devices: Recent Advances and Outlook,” *IEEE Journal of Microwaves*, vol. 1, no. 2, pp. 601–609, 2021.
 - [15] G. Giribaldi, L. Colombo, and M. Rinaldi, “6-20 GHz 30% ScAlN Lateral Field-Excited Cross-sectional Lamé Mode Resonators for future mobile RF Front-Ends,” *IEEE Trans Ultrason Ferroelectr Freq Control*, 2023.
 - [16] M. Assylbekova *et al.*, “Aluminum Nitride Combined Overtone Resonator for Millimeter Wave 5g Applications,” in *Proceedings of the IEEE International Conference on Micro Electro Mechanical Systems (MEMS)*, 2021.
 - [17] S. Nam *et al.*, “A mm-Wave Trilayer AlN/ScAlN/AlN Higher Order Mode FBAR,” *IEEE Microwave and Wireless Technology Letters*, vol. 33, no. 6, 2023.
 - [18] W. Zhao *et al.*, “15-GHz Epitaxial AlN FBARs on SiC Substrates,” *IEEE Electron Device Letters*, p. 1, 2023.
 - [19] Z. Schaffer *et al.*, “A Solidly Mounted 55 GHz Overmoded Bulk Acoustic Resonator,” in *2023 IEEE International Ultrasonics Symposium (IUS)*, 2003.
 - [20] Cho S *et al.*, “Millimeter Wave Thin-Film Bulk Acoustic Resonator in Sputtered Scandium Aluminum Nitride,” *Journal of Microelectromechanical Systems*, 2023.
 - [21] R. Vetury *et al.*, “A Manufacturable AlScN Periodically Polarized Piezoelectric Film Bulk Acoustic Wave Resonator (AlScN P3F BAW) Operating in Overtone Mode at X and Ku Band,” in *IEEE MTT-S International Microwave Symposium Digest*, 2023.
 - [22] S. Cho *et al.*, “55.4 GHz Bulk Acoustic Resonator in Thin-Film Scandium Aluminum Nitride,” in *2023 IEEE International Ultrasonics Symposium (IUS)*, 2023, pp. 1–4.
 - [23] G. Piazza, P. J. Stephanou, and A. P. Pisano, “Piezoelectric aluminum nitride vibrating contour-mode MEMS resonators,” *Journal of Microelectromechanical Systems*, vol. 15, no. 6, 2006.
 - [24] G. Piazza *et al.*, “Piezoelectric aluminum nitride thin-films for microelectromechanical systems,” *MRS Bulletin*, vol. 37, no. 11, 2012. doi: 10.1557/mrs.2012.268.
 - [25] M. Kadota and T. Ogami, “5.4 GHz Lamb wave resonator on LiNbO₃ thin crystal plate and its application,” *Jpn J Appl Phys*, vol. 50, no. 7 PART 2, 2011.
 - [26] M. Aljoumayly *et al.* “5G BAW Technology: Challenges and Solutions,” in *2022 IEEE 22nd Annual Wireless and Microwave Technology Conference, WAMICON 2022*, 2022.
 - [27] Y. Yang, A. Gao, R. Lu, and S. Gong, “5 GHz lithium niobate MEMS resonators with high FoM of 153,” in *Proceedings of the IEEE International Conference on Micro Electro Mechanical Systems (MEMS)*, 2017.
 - [28] R. Lu *et al.*, “Al resonators in 128° Y-cut Lithium Niobate with Electromechanical Coupling of 46.4%,” *Journal of Microelectromechanical Systems*, 2020.
 - [29] J. Kramer *et al.*, “57 GHz Acoustic Resonator with k₂ of 7.3 % and Q of 56 in Thin-Film Lithium Niobate,” in *IEEE International Electron Devices Meeting (IEDM)*, 2022, pp. 16.4.1–16.4.4.
 - [30] J. Kramer *et al.*, “Thin-Film Lithium Niobate Acoustic Resonator with High Q of 237 and k₂ of 5.1% at 50.74 GHz,” in *IEEE International Frequency Control Symposium (IFCS)*, 2023.
 - [31] O. Barrera *et al.*, “Thin-Film Lithium Niobate Acoustic Filter at 23.5 GHz with 2.38 dB IL and 18.2% FBW,” *Journal of Microelectromechanical Systems*, Jul. 2023.
 - [32] A. Kochhar *et al.*, “X-band Bulk Acoustic Wave Resonator (XBAW) using Periodically Polarized Piezoelectric Films (P3F),” in *2023 IEEE International Ultrasonics Symposium (IUS)*, 2023, pp. 1–4.

CONTACT

Omar Barrera, omarb@utexas.edu